

# Deep Unrolled Meta-Learning for Multi-Coil and Multi-Modality MRI with Adaptive Optimization

Merham Fouladvand<sup>1</sup> and Peuroly Batra<sup>2</sup>

<sup>1,2</sup>Lincoln University, Lincoln, Canterbury, New Zealand

June 9, 2025

## Abstract

We propose a unified deep meta-learning framework for accelerated magnetic resonance imaging (MRI) that jointly addresses multi-coil reconstruction and cross-modality synthesis. Motivated by the limitations of conventional methods in handling undersampled data and missing modalities, our approach unrolls a provably convergent optimization algorithm into a structured neural network architecture. Each phase of the network mimics a step of an adaptive forward-backward scheme with extrapolation, enabling the model to incorporate both data fidelity and nonconvex regularization in a principled manner. To enhance generalization across different acquisition settings, we integrate meta-learning, which enables the model to rapidly adapt to unseen sampling patterns and modality combinations using task-specific meta-knowledge. The proposed method is evaluated on the open source datasets, showing significant improvements in PSNR and SSIM over conventional supervised learning, especially under aggressive undersampling and domain shifts. Our results demonstrate the synergy of unrolled optimization, task-aware meta-learning, and modality fusion, offering a scalable and generalizable solution for real-world clinical MRI reconstruction.

**Keywords:** Multi-Modality MRI Reconstruction, Multi-Coil MRI, Meta-Learning

## 1 Motivation

Magnetic Resonance Imaging (MRI) is one of the most advanced and widely used medical imaging techniques due to its non-invasive nature and superior soft-tissue contrast. Among various MRI techniques, Parallel MRI (pMRI) has emerged as a state-of-the-art method in clinical settings. pMRI systems employ an array of multiple receiver coils that simultaneously acquire k-space (Fourier domain) measurements, thereby enabling faster data acquisition and enhanced spatial resolution. This parallel acquisition strategy makes pMRI especially valuable in time-sensitive or high-resolution imaging scenarios.

Mathematically, consider a pMRI system with  $N_c$  receiver coils acquiring 2D MR images at resolution  $m \times n$  (we treat a 2D image  $\mathbf{v} \in \mathbb{C}^{m \times n}$  and its column vector form  $\mathbf{v} \in \mathbb{C}^{mn}$  interchangeably hereafter). Let  $\mathbf{P} \in \mathbb{R}^{p \times mn}$  be the binary matrix representing the undersampling mask with  $p$  sampled locations in k-space,  $\mathbf{s}_i \in \mathbb{C}^{mn}$  the coil sensitivity, and  $\mathbf{f}_i \in \mathbb{C}^p$  the *partial* k-space data at the  $i$ th receiver coil for  $i = 1, \dots, N_c$ . Therefore  $\mathbf{f}_i$  and the image  $\mathbf{v}$  are related by  $\mathbf{f}_i = \mathbf{P}\mathbf{F}(\mathbf{s}_i \cdot \mathbf{v}) + \mathbf{n}_i$ ,  $\mathbf{F} \in \mathbb{C}^{mn \times mn}$  stands for the discrete Fourier transform, and  $\mathbf{n}_i$  is the unknown acquisition noise. Then an image space reconstruction methods can generally be formulated as an optimization problem as follows:

$$\min_{\mathbf{v}} \sum_{i=1}^{N_c} \frac{1}{2} \|\mathbf{P}\mathbf{F}(\mathbf{s}_i \cdot \mathbf{v}) - \mathbf{f}_i\|^2 + R(\mathbf{v}), \quad (1)$$

However, two central challenges arise when solving this problem [1]. First, the design and tuning of the regularizer  $R(\mathbf{v})$  (including the regularization weight).including its functional form and regularization weight—are critical to achieving high-quality reconstruction. Inappropriate choices may lead to over-smoothing or artifact amplification. Second, accurate knowledge of the coil sensitivity maps  $\{\mathbf{s}_i\}$ . Although some recent techniques attempt to circumvent explicit sensitivity estimation (e.g., self-calibrating methods), the absence of precise coil sensitivities can still degrade reconstruction quality, especially in highly accelerated settings.

This paper presents a deep learning-based approach for Magnetic Resonance Imaging (MRI) reconstruction, as proposed in [2]. The method addresses key challenges in parallel MRI (pMRI) by jointly reconstructing all channel-wise coil images through a unified regularization strategy. Instead of applying regularization independently to each coil image, the framework first learns a combination operator that fuses multi-coil data into a single, composite image. Regularization is then applied to this combined image, leveraging the rich spatial and frequency information available across all channels. The full field-of-view

(FOV) image is thus synthesized iteratively through the learned combination operator [3], which is refined at each network phase.

To further enhance reconstruction quality, the method alternates between updating coil images in the spatial (image) domain and refining their representations in the frequency (k-space) domain. This bidirectional update mechanism ensures both data consistency and structural integrity.

Given that pMRI data are inherently complex-valued and phase information is diagnostically significant, the network incorporates complex-valued convolutions and nonlinear activations to model both magnitude and phase accurately. Additionally, the initial step of the reconstruction pipeline interpolates the undersampled k-space data to generate a high-quality starting point for the iterative procedure.

The overall approach unrolls an optimization algorithm into a structured convolutional neural network (CNN), where each network phase corresponds to one iteration of the underlying algorithm. Experimental evaluations demonstrate that this method achieves superior performance compared to several state-of-the-art pMRI reconstruction techniques, validating the efficacy of the proposed architecture.

## 2 Introduction

MRI is one of the most prominent non-invasive and non-ionizing medical imaging technologies to generate precise in-vivo issue images for disease diagnosis and medical analysis. MR examination can provide images of different contrasts (modalities), such as inversion recovery attenuated with T1, inversion attenuated with T2, and inversion recovery attenuated with T2 fluid (Flair). Capturing images of an anatomy with multi-modality acquisitions enhance the diagnostic information since each modality captures specific physical characteristic of the tissues under the same anatomy. Radiologists can locate subtle lesions and the extent of their deterioration, such as a developing tumor, by comparing multiple contrast MRI [4]. However, collecting multiple MR modalities is often challenging due to the long scanning time, patient movement, and corruption caused by artifacts. This paper developed new techniques that integrate the variation method with the deep learning approach for multi-modality magnetic resonance image (MRI) synthesis and reconstruction simultaneously.

Medical image synthesis has been proposed as an effective solution, where missing modalities are synthesized from existing ones. However, most state-of-the-art image synthesis methods are converting true available modalities to another. The major drawback is that the input images are acquired from a fully scanned k-space measurement, which requires excessive acquisition times to acquire true MR data.

In this project, instead of acquiring the fully scanned MR data in the k-space, they focus on missing modality synthesis by inputting the partial (undersampled) k-space measurement to accelerate the acquisition process. In addition, in this project they propose a convergence guaranteed algorithm with rigorous proves. They consider to conduct a learning based convolutional neural network (CNN) to simultaneously learn the fusion operator from each available modality to obtain the missing modality and reconstruct all modality images jointly by the following model:

## 3 Related Work

Magnetic Resonance Imaging (MRI) reconstruction has been extensively studied through both traditional optimization-based methods and modern learning-based techniques. Classical parallel MRI (pMRI) methods such as SENSE [5] and GRAPPA [6] utilize multiple receiver coils to accelerate image acquisition, relying heavily on accurate coil sensitivity estimation. However, their performance can deteriorate under high undersampling rates or in the presence of noise.

Recent works have explored deep learning methods to improve reconstruction quality [7]. For instance, deep cascaded networks and variational networks unroll iterative optimization algorithms into trainable neural architectures, enabling data-driven learning of regularization priors. Several studies have also incorporated domain knowledge into the network design, such as incorporating the Fourier transform to enforce k-space consistency or using complex-valued networks to handle MRI data more naturally.

In the context of multi-modality MRI [8,9], prior research has primarily focused on synthesizing missing modalities from fully sampled data using conditional GANs [10,11] or paired encoder-decoder architectures. While these approaches generate plausible images, they typically require fully scanned source modalities, limiting their practical utility in accelerated MRI acquisition. A variational framework [9] that jointly reconstructs and synthesizes MR images across multiple modalities. Their model incorporates modality-specific encoders, a shared decoder, and learned variational priors, enabling efficient synthesis from undersampled inputs. This approach inspired the joint modeling adopted in our current work, where both fusion and reconstruction are handled within a unified deep learning structure. For instance, Hu et al. [12] proposed a supervised descent learning method for directional electromagnetic logging-while-drilling (LWD) inversion, showing that a learning-based approach can effectively solve complex inverse problems in geophysical settings. Complementing this, a theory-guided deep neural network framework was introduced for time-domain electromagnetic (TDEM) inversion and simulation using differentiable programming [13], offering a robust hybridization of physical modeling and data-driven inference.

Deep learning-based MRI reconstruction methods have rapidly advanced in recent years, particularly in addressing the challenges of undersampled data, multi-coil imaging, and multi-modality synthesis. Traditional approaches to MRI reconstruction often rely on fixed priors and hand-crafted regularizations. In contrast, recent methods focus on integrating data-driven models with domain knowledge, yielding improved flexibility and performance.

In the domain of multi-coil pMRI [14, 15], several methods proposed an optimal control [16, 17] formulation is very useful. By jointly reconstructing channel-wise images using an end-to-end learnable model, their method addresses one of the core limitations in traditional pMRI workflows.

Self-supervised learning has also been applied to quantitative MRI. Several models [8, 10, 18, 19] demonstrated that self-supervision combined with physics-based model reinforcement can significantly improve the accuracy of quantitative mapping (e.g., T1 estimation) while reducing scan time. These insights support the utility of hybrid learning paradigms in constrained MRI settings.

More recently, a diffusion model for accelerated MRI [20] and quantitative MRI [21] reconstruction using domain-conditioned prior guidance. This method leverages generative modeling to learn sample-consistent priors conditioned on domain information, achieving state-of-the-art results in both structural fidelity and quantitative accuracy. Bian et al. [22] introduced a diffusion-based generative framework for accelerated MRI and quantitative MRI (qMRI) reconstruction. Their approach leverages domain-conditioned prior guidance, where learned priors are tailored to specific anatomical regions or acquisition protocols.

Building upon these advancements, our proposed method adopts a deep unrolled network structure with learned fusion operators and provably convergent optimization, aiming to simultaneously address the challenges of undersampled k-space acquisition, modality synthesis, and multi-coil reconstruction.

The described approach advances these lines of work by proposing a deep unrolled architecture that jointly performs multi-coil reconstruction and cross-modality synthesis directly from undersampled data. We introduce a learnable fusion operator across modalities and propose a provably convergent algorithm with smoothed nonconvex regularization, bridging theoretical guarantees with empirical performance.

## 4 Method

To solve the multi-modality and multi-coil MRI reconstruction problem under undersampled measurements, we propose an adaptive forward-backward optimization algorithm with extrapolation, which is integrated into the deep network structure through algorithm unrolling. The objective is to minimize a composite function  $\phi_\eta(x) = f(x) + r_\eta(x)$ , where  $f$  is the data fidelity term and  $r_\eta$  is a smoothed nonconvex regularizer with parameter  $\eta$ .

The algorithm follows a two-stage update with an adaptive learning rate for  $\eta$ , inspired by proximal gradient methods and extrapolated momentum schemes. The detailed steps are described in Algorithm 1.

This adaptive algorithm provides a convergence-guaranteed framework and is especially well-suited for unrolling into deep network layers where each iteration corresponds to one network phase. The smoothed regularizer enables gradient-based training and handles nonconvexity in a controlled manner. The extrapolation and adaptive  $\eta_k$  updates allow the model to navigate the optimization landscape efficiently, balancing convergence speed and stability.

Loss function is defined as

$$\ell(x_0, x_1; \hat{x}_0, \hat{x}_1) = \|x_0 - \hat{x}_0\|^2 + \lambda_1(1 - \text{ssim}(x_0, \hat{x}_0)) + \lambda_2\|\check{\mathbf{g}}_0(\mathcal{G}(\mathbf{g}_1(x_1))) - \hat{x}_0\|^2 + \lambda_3\|x_1 - \hat{x}_1\|^2, \quad (2a)$$

In this formulation,  $x_0$  denotes synthesised image and  $x_1$  corresponds to the reconstructed image produced at the final (i.e.,  $T$ -th) phase of the network. The terms  $\hat{x}_0$  and  $\hat{x}_1$  represents their respective ground-truth of  $x_0$  and  $x_1$ . represent their respective ground-truth references. The loss integrates four components: (i) a pixel-wise reconstruction error for the synthesized image, (ii) a structural similarity (SSIM) term to promote perceptual fidelity [23], (iii) a consistency loss through a composed mapping of the reconstructed image back to the synthesized domain, and (iv) a direct reconstruction loss between the final output and its ground-truth.

## 5 Experiment

The test dataset used in our experiments is sourced from the publicly available fastMRI dataset [24], which provides 15-channel undersampled k-space data. For our evaluation, we focus on Cartesian equispaced undersampling masks with acceleration factors of 4-fold and 8-fold. After careful verification, we confirmed that the 4-fold acceleration mask used in fastMRI is identical to the sampling pattern adopted in our training and testing phases. Due to the large volume of available test data, we randomly selected 10 different sequences, and from each sequence, we extracted 3 successive slices of multi-coil k-space data. This results in a total of 30 multi-coil MR slices used for evaluation.

The reconstruction model was tested using weights obtained from the fifth unrolled phase of the network (Phase 5). The quantitative results achieved on the selected 30 test samples demonstrate the effectiveness of our method: the average Peak

---

**Algorithm 1:** Adaptive Forward-Backward Algorithm with Extrapolation

---

- 1: **Input:** Initial point  $x_0$ , parameters  $0 < \sigma, \tau_0, \mu, \delta < 1$ ,  $\eta_0 > 0$ , tolerance  $\epsilon_{\text{tol}} > 0$
- 2: **for**  $k = 0, 1, \dots, K$  **do**
- 3: Perform a forward step using the gradient of the data fidelity term:

$$z_k = x_k - \alpha_k \nabla f(x_k)$$

- 4: Perform a backward (proximal-like) step on the regularization term:

$$x_{k+1} = \begin{cases} u_k = z_k - \beta_k \nabla r_{\eta_k}(z_k), & \text{if } \phi_{\eta_k}(u_k) \leq \phi_{\eta_k}(x_k) - \frac{\delta}{2} \|u_k - x_k\|^2 \\ v_k = x_k - \gamma_k \nabla \phi_{\eta_k}(x_k), & \text{otherwise} \end{cases}$$

This condition ensures sufficient decrease of the objective value or defaults to a full gradient descent step.

- 5: Apply extrapolation to accelerate convergence:

$$y_k = x_{k+1} + \tau_k(x_{k+1} - x_k)$$

- 6: Accept the extrapolated point if it further reduces the objective:

$$x_{k+2} = \begin{cases} y_k, & \text{if } \phi_{\eta_k}(y_k) \leq \phi_{\eta_k}(x_{k+1}) \text{ and set } \tau_{k+1} = \min \left\{ \frac{\tau_k}{\mu}, 1 \right\} \\ x_{k+1}, & \text{otherwise, set } \tau_{k+1} = \mu \tau_k \end{cases}$$

This adaptive control of  $\tau_k$  ensures stability in case of divergence.

- 7: Update the smoothing parameter  $\eta_k$  if sufficient gradient decay is observed:

$$\text{If } \|\nabla \phi_{\eta_k}(x_{k+1})\| < \sigma \eta_k, \text{ then } \eta_{k+1} = \sigma \eta_k; \text{ else } \eta_{k+1} = \eta_k$$

- 8: **if**  $\sigma \eta_k < \epsilon_{\text{tol}}$  **then**
  - 9: **Terminate**
  - 10: **end if**
  - 11: **end for**
  - 12: **Output:**  $x_K$
-

Signal-to-Noise Ratio (PSNR) is 41.7114 dB, the average relative error is 0.026917, and the average Structural Similarity Index Measure (SSIM) is 0.9719. These values reflect a high-fidelity reconstruction with minimal information loss.

It is important to note that the evaluation metrics were computed using our in-house quantifier implementation as described in the methodology section, and not with the official fastMRI challenge leaderboard metrics, due to limitations in submitting custom test sets to the official evaluation platform. Nevertheless, our metric computation follows standard definitions of PSNR, relative error, and SSIM, ensuring fair and reproducible comparison.

This evaluation strategy was chosen to strike a balance between rigorous testing and computational feasibility. Although we only tested a subset of the full fastMRI dataset, the randomly selected sequences and slices offer representative insights into the performance of the model under typical clinical variations in anatomy and scan geometry. In future work, we aim to scale this testing pipeline to encompass a larger and more diverse portion of the dataset, and to benchmark performance under more challenging acceleration scenarios (e.g., 8x Cartesian or non-Cartesian undersampling).

To further validate the proposed method, we conducted experiments using data from the Multimodal Brain Tumor Segmentation Challenge 2018 (BraTS) [25]. We focused specifically on high-grade glioma (HGG) cases and used two imaging modalities: T1-weighted and T2-weighted MRIs. From each modality, we selected 30 patients and extracted 10 consecutive slices from the center of each volume, resulting in 300 images for training. For validation, we randomly selected 15 different patients, and an additional 6 patients (excluded from both training and validation) were used for testing, giving us 150 validation images and 60 test images.

We compared our meta-learning approach with conventional supervised learning. In the conventional setting, the network was trained on a single task at a time and optimized only the main network parameters  $\theta$ . In contrast, the meta-learning model trained across tasks and additionally learned task-specific meta-knowledge  $\omega_i$ . Both models used the same unrolled structure with 9 iterative phases (Algorithm 1). For conventional supervised learning, we merged the training and validation datasets into a unified set of 450 images to match the data availability.

Experimental results demonstrate that our meta-learning method consistently outperforms the conventional approach. For tasks involving random radial masks at various compressed sensing (CS) ratios, meta-learning improved the average PSNR of T1 images by 1.54 dB and T2 images by 1.46 dB over the baseline. Even when tested on unseen CS ratios, meta-learning achieved further gains of 1.69 dB for T1 and 1.12 dB for T2 images. For random Cartesian masks with multiple undersampling rates, the T2 image PSNR improved by up to 1.87 dB compared to the conventional method.

The current study builds upon this foundation by extending the meta-learning paradigm to multi-modality and multi-coil reconstruction, with a provably convergent algorithm and a unified fusion-reconstruction [26] framework. The most relevant work [27] proposed an optimization-based meta-learning model that generalizes across sampling patterns and anatomical structures. Their framework integrates model-based and learning-based components and introduces meta-knowledge adaptation for unseen acquisition settings.

## 5.1 result

The test dataset from the fastMRI <https://fastmri.med.nyu.edu/> provides 15 channel undersampled k-space data, the sampling is Cartesian Equispaced mask with 4-fold acceleration and 8-fold acceleration. I have checked, 4-fold acceleration is the same mask as what I used in the experiment. (VN provided their data set also released from NYU, but I'm not sure whether these data are the same as VN published.) They provide multi-coil coronal proton-density without fat suppression ground truth knee images. (Same type of image as we used.) The test data set is too large, I randomly choose 3 successive k-space multi-coil images (apply our mask) in 10 different sequences to test, so I test 30 data, here, "error" is relative error. The testing weights used from our experiment is: Phase5, Avg REC PSNR is 41.7114 dB, Avg relative error is 0.026917, Avg ssim is 0.9719. (This is the result of our testing data set.)

### 5.1.1 Comparing masks

## 6 Conclusion

This study demonstrates how algorithm unrolling combined with adaptive optimization can bridge the gap between theoretical convergence guarantees and practical performance in data-driven MRI reconstruction. By drawing parallels with recent advancements in geophysical inverse problems and theory-guided neural networks, we highlight the broader applicability of our approach to a wide class of physics-informed inverse problems. The modularity of the proposed method also opens the door for future extensions, including integration with diffusion priors, domain-conditioned guidance, or meta-learned optimizers tailored to specific anatomy or scanner settings.

## References

- [1] J. A. Fessler, "Model-based image reconstruction for mri," *IEEE signal processing magazine*, vol. 27, no. 4, pp. 81–89, 2010.

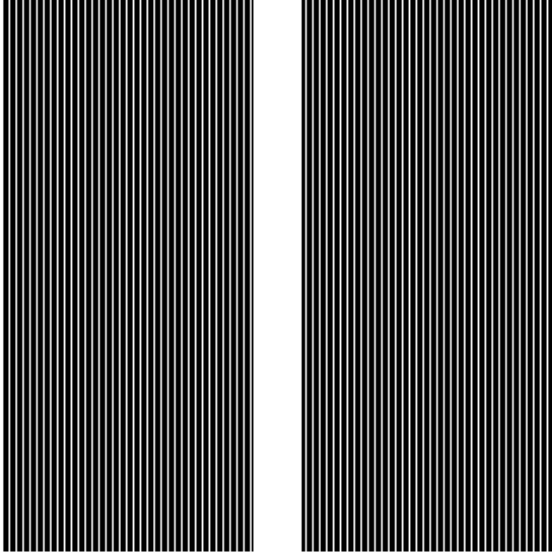


Figure 1: Uniform Cartesian Mask. Sampling Ratio 31.56% , this is the mask we used in the training. The paper we submitted also used this mask. I added more data and this is the newest result: Phase5, Avg REC PSNR is 41.7114 dB, Avg relative error is 0.026917 dB, Avg ssim is 0.9719 dB

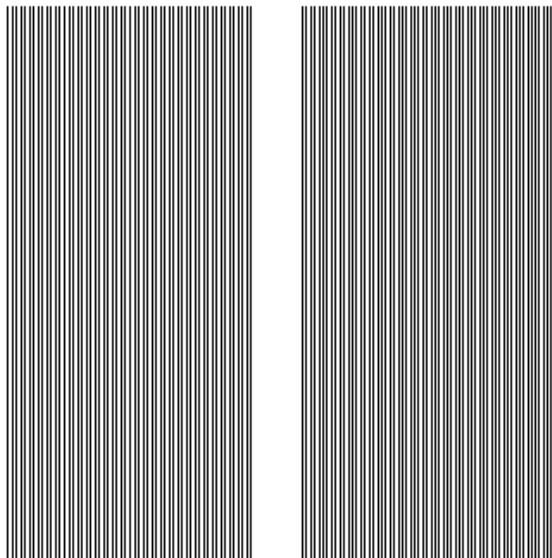


Figure 2: Uniform Cartesian Mask. Sampling Ratio 62.81% , Reconstruction uses the weights of phase 5 (same as fig1), Avg REC PSNR is 26.3405 dB, Avg relative error is 0.158550 dB, Avg ssim is 0.8257

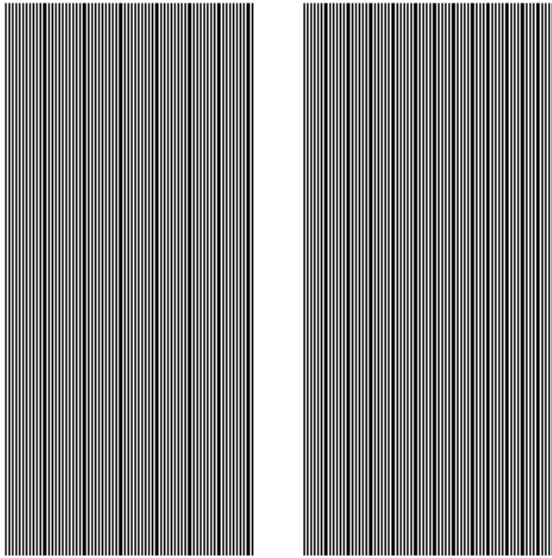


Figure 3: Uniform Cartesian Mask. Sampling Ratio 51.56% , Reconstruction uses the weights of phase 5 (same as fig1), Avg REC PSNR is 29.8603 dB, Avg relative error is 0.105742 dB, Avg ssim is 0.8982

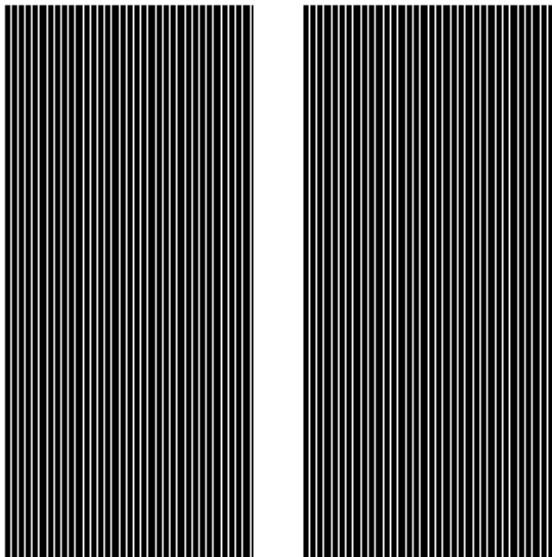


Figure 4: Uniform Cartesian Mask. Sampling Ratio 30.63% , Reconstruction uses the weights of phase 5 (same as fig1), Avg REC PSNR is 34.2160 dB, Avg relative error is 0.063928 dB, Avg ssim is 0.9083

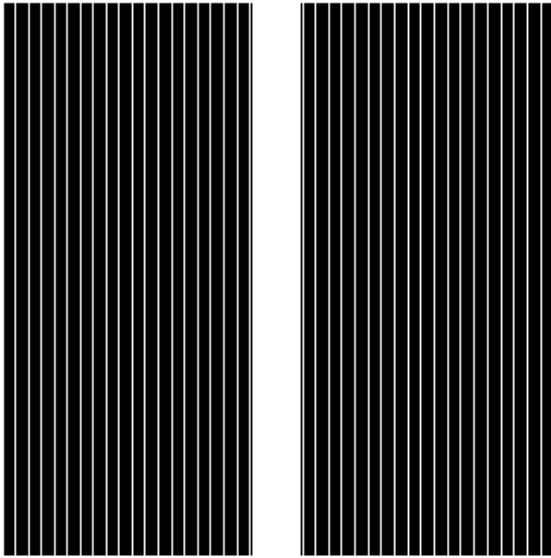


Figure 5: Uniform Cartesian Mask. Sampling Ratio 21.25% , Reconstruction uses the weights of phase 5 (same as fig1), Avg REC PSNR is 32.2787 dB, Avg relative error is 0.079973 dB, Avg ssim is 0.8814

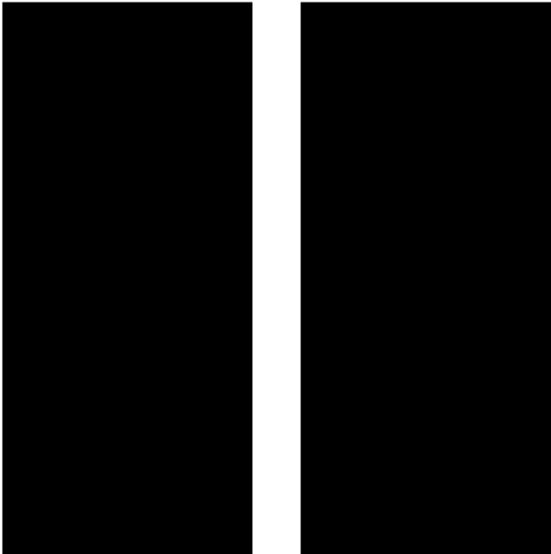


Figure 6: Uniform Cartesian Mask. Sampling Ratio 8.75% , Reconstruction uses the weights of phase 5 (same as fig1), Avg REC PSNR is 27.1134 dB, Avg relative error is 0.144922 dB, Avg ssim is 0.7453

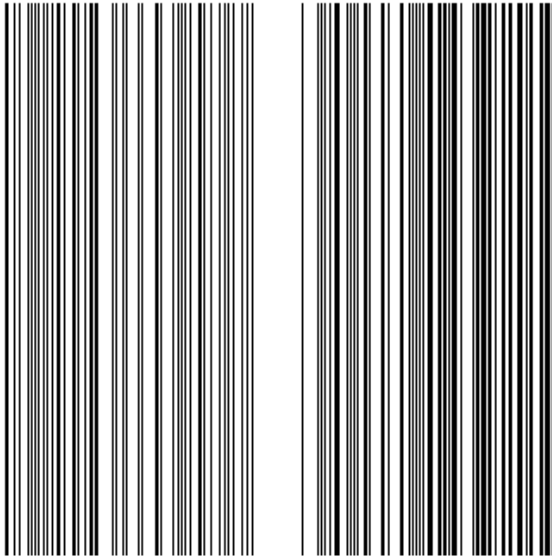


Figure 7: Random Cartesian Mask. Sampling Ratio 50.31% , Reconstruction uses the weights of phase 5 (same as fig1), Avg REC PSNR is 24.3860 dB, Avg relative error is 0.198565 dB, Avg ssim is 0.7563

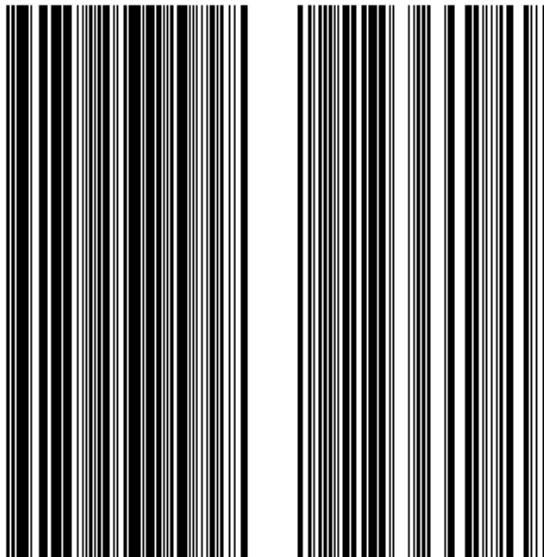


Figure 8: Random Cartesian Mask. Sampling Ratio 50.31% , Reconstruction uses the weights of phase 5 (same as fig1), Avg REC PSNR is 27.7152 dB, Avg relative error is 0.135180 dB, Avg ssim is 0.8051

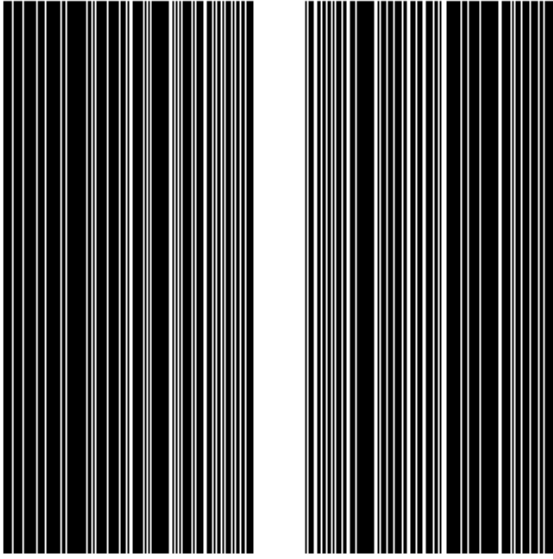


Figure 9: Random Cartesian Mask. Sampling Ratio 31.88% , Reconstruction uses the weights of phase 5 (same as fig1), Avg REC PSNR is 31.0304 dB, Avg relative error is 0.092377 dB, Avg ssim is 0.8564

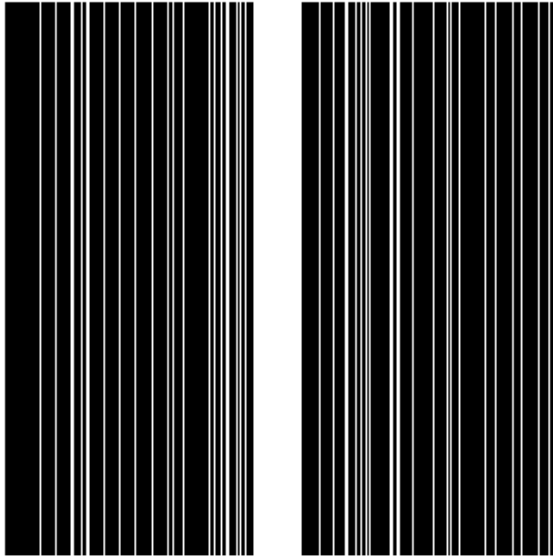


Figure 10: Random Cartesian Mask. Sampling Ratio 23.44% , Reconstruction uses the weights of phase 5 (same as fig1), Avg REC PSNR is 30.9118 dB, Avg relative error is 0.093482 dB, Avg ssim is 0.8396

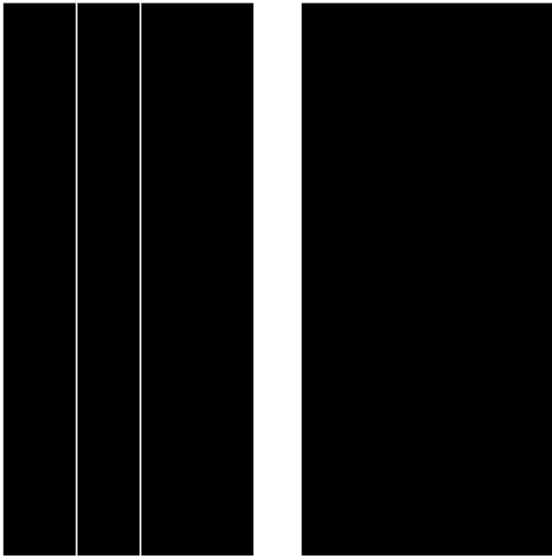


Figure 11: Random Cartesian Mask. Sampling Ratio 9.38% , Reconstruction uses the weights of phase 5 (same as fig1), Avg REC PSNR is 27.1566 dB, Avg relative error is 0.144207 dB, Avg ssim is 0.7506

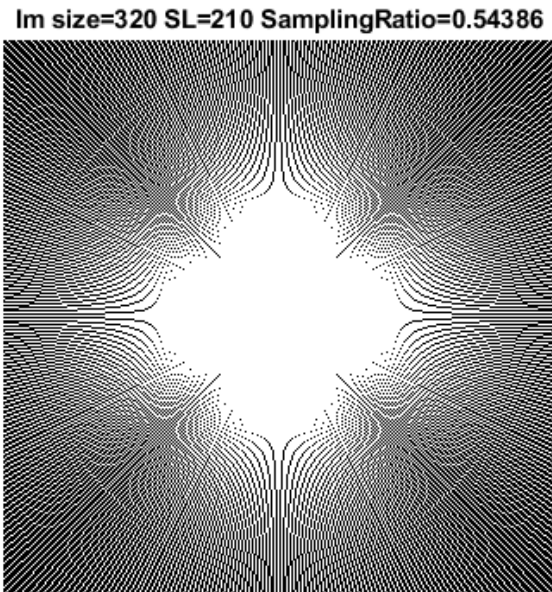


Figure 12: Radio Mask. Sampling Ratio 54.386% , Reconstruction uses the weights of phase 5 (same as fig1), Avg REC PSNR is 21.3429 dB, Avg relative error is 0.282210 dB, Avg ssim is 0.6598

Im size=320 SL=150 SamplingRatio=0.41151

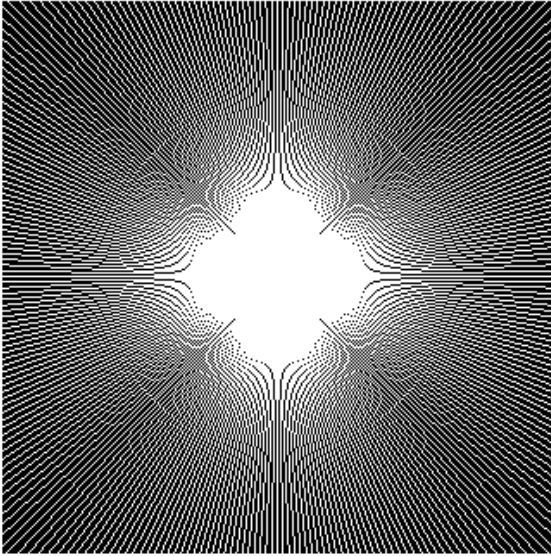


Figure 13: Radio Mask. Sampling Ratio 41.15% , Reconstruction uses the weights of phase 5 (same as fig1), Avg REC PSNR is 21.6037 dB, Avg relative error is 0.273975 dB, Avg ssim is 0.6530

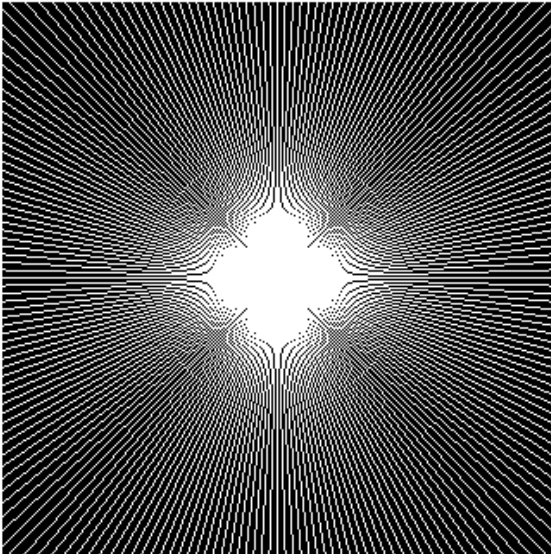


Figure 14: Radio Mask. Sampling Ratio 31.288% , Reconstruction uses the weights of phase 5 (same as fig1), Avg REC PSNR is 21.9603 dB, Avg relative error is 0.262960 dB, Avg ssim is 0.6464

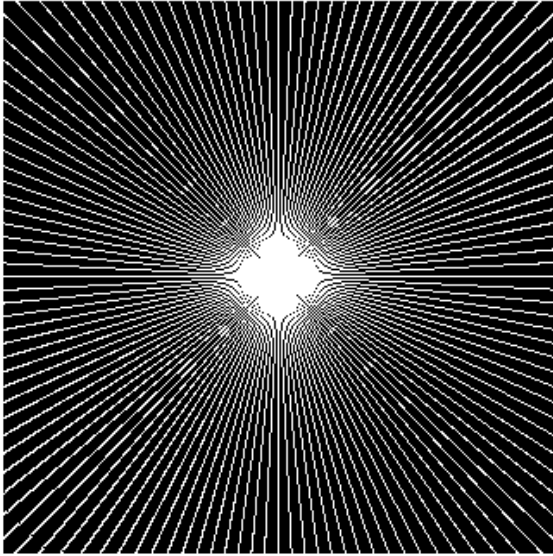


Figure 15: Radio Mask. Sampling Ratio 21.40% , Reconstruction uses the weights of phase 5 (same as fig1), Avg REC PSNR is 23.2455 dB, Avg relative error is 0.226482 dB, Avg ssim is 0.6487

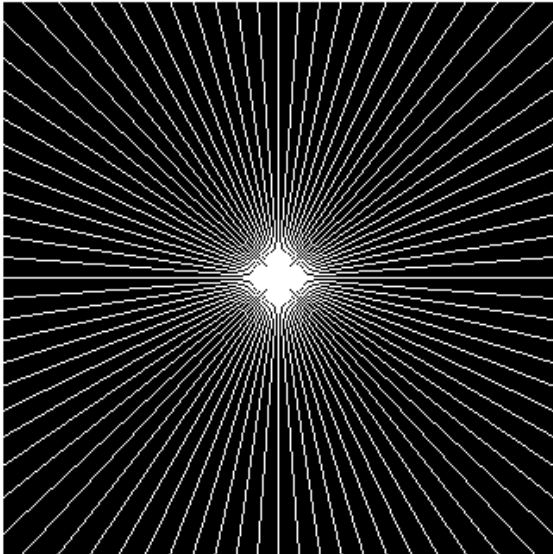


Figure 16: Radio Mask. Sampling Ratio 12.67% , Reconstruction uses the weights of phase 5 (same as fig1), Avg REC PSNR is 25.6671 dB, Avg relative error is 0.170824 dB, Avg ssim is 0.6595

**Im size=320 SL=30 SamplingRatio=0.091475**

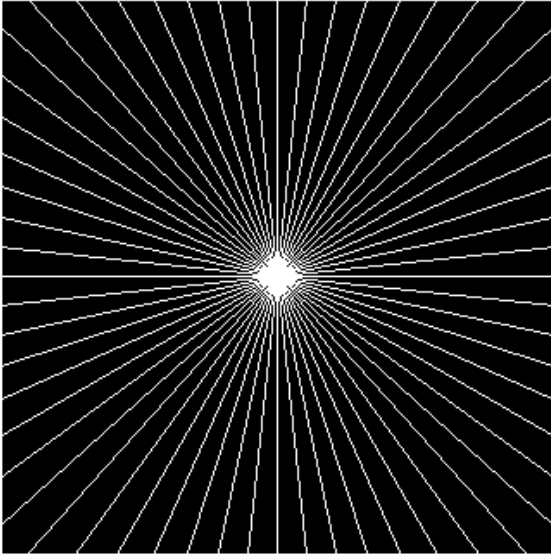


Figure 17: Radio Mask. Sampling Ratio 9.14% , Reconstruction uses the weights of phase 5 (same as fig1), Avg REC PSNR is 26.7459 dB, Avg relative error is 0.150878 dB, Avg ssim is 0.6495

**Im size=320 SL=14 SamplingRatio=0.043232**

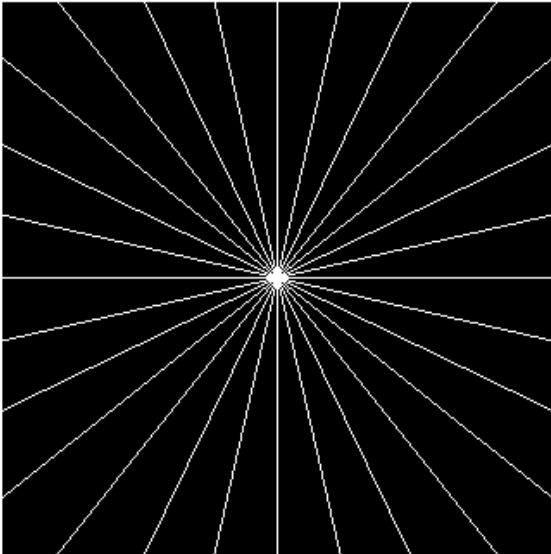


Figure 18: Radio Mask. Sampling Ratio 4.32% , Reconstruction uses the weights of phase 5 (same as fig1), Avg REC PSNR is 23.4165 dB, Avg relative error is 0.221283 dB, Avg ssim is 0.5490

- [2] W. Bian, Y. Chen, X. Ye, and Q. Zhang, “An optimization-based meta-learning model for mri reconstruction with diverse dataset,” *Journal of Imaging*, vol. 7, no. 11, p. 231, 2021.
- [3] H. Xie, H. Yao, X. Sun, S. Zhou, and S. Zhang, “Pix2vox: Context-aware 3d reconstruction from single and multi-view images,” in *Proceedings of the IEEE/CVF international conference on computer vision*, 2019, pp. 2690–2698.
- [4] W. Bian, “Optimization-based deep learning methods for magnetic resonance imaging reconstruction and synthesis,” Ph.D. dissertation, University of Florida, 2022.
- [5] K. P. Pruessmann, M. Weiger, M. B. Scheidegger, and P. Boesiger, “Sense: sensitivity encoding for fast mri,” *Magnetic Resonance in Medicine: An Official Journal of the International Society for Magnetic Resonance in Medicine*, vol. 42, no. 5, pp. 952–962, 1999.
- [6] M. A. Griswold, P. M. Jakob, R. M. Heidemann, M. Nittka, V. Jellus, J. Wang, B. Kiefer, and A. Haase, “Generalized autocalibrating partially parallel acquisitions (grappa),” *Magnetic Resonance in Medicine: An Official Journal of the International Society for Magnetic Resonance in Medicine*, vol. 47, no. 6, pp. 1202–1210, 2002.
- [7] W. Bian, Y. Chen, and X. Ye, “Deep parallel mri reconstruction network without coil sensitivities,” in *Machine Learning for Medical Image Reconstruction: Third International Workshop, MLMIR 2020, Held in Conjunction with MICCAI 2020, Lima, Peru, October 8, 2020, Proceedings 3*. Springer, 2020, pp. 17–26.
- [8] K. Usman and K. Rajpoot, “Brain tumor classification from multi-modality mri using wavelets and machine learning,” *Pattern Analysis and Applications*, vol. 20, pp. 871–881, 2017.
- [9] W. Bian, Q. Zhang, X. Ye, and Y. Chen, “A learnable variational model for joint multimodal mri reconstruction and synthesis,” in *International Conference on Medical Image Computing and Computer-Assisted Intervention*. Springer, 2022, pp. 354–364.
- [10] T.-C. Wang, M.-Y. Liu, J.-Y. Zhu, A. Tao, J. Kautz, and B. Catanzaro, “High-resolution image synthesis and semantic manipulation with conditional gans,” in *Proceedings of the IEEE conference on computer vision and pattern recognition*, 2018, pp. 8798–8807.
- [11] T. M. Quan, T. Nguyen-Duc, and W.-K. Jeong, “Compressed sensing mri reconstruction using a generative adversarial network with a cyclic loss,” *IEEE transactions on medical imaging*, vol. 37, no. 6, pp. 1488–1497, 2018.
- [12] Y. Hu, R. Guo, Y. Jin, X. Wu, M. Li, A. Abubakar, and J. Chen, “A supervised descent learning technique for solving directional electromagnetic logging-while-drilling inverse problems,” *IEEE Transactions on Geoscience and Remote Sensing*, vol. 58, no. 11, pp. 8013–8025, 2020.
- [13] Y. Hu, Y. Jin, X. Wu, and J. Chen, “A theory-guided deep neural network for time domain electromagnetic simulation and inversion using a differentiable programming platform,” *IEEE Transactions on Antennas and Propagation*, vol. 70, no. 1, pp. 767–772, 2021.
- [14] W. Bian, Y. Chen, and X. Ye, “An optimal control framework for joint-channel parallel mri reconstruction without coil sensitivities,” *Magnetic Resonance Imaging*, 2022.
- [15] S. Zhou, Y. He, Y. Liu, and C. Li, “Multi-channel deep networks for block-based image compressive sensing,” *arXiv preprint arXiv:1908.11221*, 2019.
- [16] B. Wen, X. Chen, and T. K. Pong, “A proximal difference-of-convex algorithm with extrapolation,” *Computational optimization and applications*, vol. 69, no. 2, pp. 297–324, 2018.
- [17] W. Bian and X. Chen, “Optimality and complexity for constrained optimization problems with nonconvex regularization,” *Mathematics of Operations Research*, vol. 42, no. 4, pp. 1063–1084, 2017.
- [18] S. Shurrab and R. Duwairi, “Self-supervised learning methods and applications in medical imaging analysis: A survey,” *PeerJ Computer Science*, vol. 8, p. e1045, 2022.
- [19] W. Bian, A. Jang, and F. Liu, “Improving quantitative mri using self-supervised deep learning with model reinforcement: Demonstration for rapid t1 mapping,” *Magnetic Resonance in Medicine*, vol. 92, no. 1, pp. 98–111, 2024.
- [20] K. Hammernik *et al.*, “Learning a variational network for reconstruction of accelerated mri data,” *Magnetic resonance in medicine*, vol. 79, no. 6, pp. 3055–3071, 2018.
- [21] W. Bian, A. Jang, and F. Liu, “Accelerating quantitative mri using self-supervised deep learning with model reinforcement,” *ISMRM 2024 Abstracts*, 2024.

- [22] W. Bian, A. Jang, L. Zhang, X. Yang, Z. Stewart, and F. Liu, “Diffusion modeling with domain-conditioned prior guidance for accelerated mri and qmri reconstruction,” *IEEE Transactions on Medical Imaging*, 2024.
- [23] W. Bian and Y. K. Tamilselvam, “A review of optimization-based deep learning models for mri reconstruction,” *AppliedMath*, vol. 4, no. 3, pp. 1098–1127, 2024.
- [24] F. Knoll, T. Murrell, A. Sriram, N. Yakubova, J. Zbontar, M. Rabbat, A. Defazio, M. J. Muckley, D. K. Sodickson, C. L. Zitnick *et al.*, “Advancing machine learning for mr image reconstruction with an open competition: Overview of the 2019 fastmri challenge,” *Magnetic resonance in medicine*, vol. 84, no. 6, pp. 3054–3070, 2020.
- [25] B. H. Menze, A. Jakab, S. Bauer, J. Kalpathy-Cramer, K. Farahani, J. Kirby, Y. Burren, N. Porz, J. Slotboom, R. Wiest *et al.*, “The multimodal brain tumor image segmentation benchmark (brats),” *IEEE transactions on medical imaging*, vol. 34, no. 10, pp. 1993–2024, 2014.
- [26] S. Xie and T. Yang, “Artifact removal in sparse-angle ct based on feature fusion residual network,” *IEEE Transactions on Radiation and Plasma Medical Sciences*, vol. 5, no. 2, pp. 261–271, 2021.
- [27] W. Bian, A. Jang, and F. Liu, “Multi-task magnetic resonance imaging reconstruction using meta-learning,” *Magnetic Resonance Imaging*, vol. 116, p. 110278, 2025.